

# Brittle-Ductile Transition in a Metallic Glass

J.S. Langer

*Kavli Institute for Theoretical Physics, Kohn Hall,  
University of California, Santa Barbara, CA 93106*

(Dated: June 11, 2019)

Recent computational and laboratory experiments have shown that the brittle-ductile transition in metallic glasses such as Vitreloy-1 is strongly sensitive to the initial effective disorder (or “fictive”) temperature. Glasses with lower effective temperatures are brittle; those with higher effective temperatures are ductile. The analysis of this phenomenon presented here starts with an elongated elliptical hole in a stressed elastic plate, and examines the onset of deformation at the tip of the ellipse as predicted by a shear-transformation-zone (STZ) theory of spatially varying plastic deformation. Agreement between theory and experiment, while necessarily limited to the onset behavior, is quite good.

## I. INTRODUCTION

Two recent developments in fracture mechanics have interesting implications for materials theory. Specifically, the numerical simulations of amorphous crack-tip dynamics by Rycroft and Bouchbinder [1], and the related experimental results for metallic glasses by Ketkaew et al.[2], both demonstrate that amorphous materials are embrittled by forming them with low densities of flow defects. Reference [1] shows that notch-like indentations sharpen and launch cracks at low effective disorder temperatures and correspondingly low initial densities of shear-transformation zones (STZ’s).[3, 4] According to Ref.[2] (see also [5]), crack formation in metallic glasses is enhanced by decreasing their fictive temperatures. That is, glasses are embrittled by quenching them slowly enough through their glass temperatures that they settle into states of relatively small disorder. Conversely, they remain tougher when quenched more quickly.

Fracture toughness is a central issue in materials science that has long been addressed primarily by phenomenology. However, we now have the STZ theory for amorphous plasticity [3, 4] and the thermodynamic dislocation theory for crystalline materials [6–8], both of which are based on fundamental nonequilibrium physics and have been successfully tested by experiment. With [1] and [2], we have simulational and experimental results directly relevant to the brittle-ductile problem. Thus the time seems ripe to look carefully at the basic theory of these phenomena to make sure we understand what is happening.

Here I describe an attempt to interpret the results of [1] and [2] analytically. My strategy is to consider a long, thin elliptical hole in a sheet of material subject to an increasing, mode-I, opening stress. I use a simple Bingham plasticity law (a special case of the STZ theory) with a linear increase in the plastic deformation rate as a function of stress above a fixed yield point; and I look only at the onset of plastic deformation at the tip of the ellipse where the stress is most highly concentrated. My one extra degree of freedom is the effective temperature which, in the STZ theory, is a measure of the density of flow defects. If the tip sharpens as I increase the stress,

then I conclude that the system is producing a crack and is brittle. Conversely, if the tip flattens, then I conclude – but with some uncertainty – that the system is ductile.

Because I am looking only at the onset of deformation, I cannot predict the measured fracture toughness. I cannot even predict whether the failure mode develops into a fast crack like those seen by Fineberg et al [9] in thin plastic strips, or a complex pattern of crack branches as seen in [1], or whether the elliptical tip advances slowly into an expanding plastic zone. At best, I can predict how the initial behavior depends on system preparation. As will be seen, I can do that quite accurately.

Even the simplest version of the Bingham analysis, without the variable effective temperature, requires approximations. But the answer is surprisingly simple. As the concentrated stress near the tip increases through the yield stress, a thin plastic boundary layer appears at the tip, within which the plastic flow is such that the tip eventually moves forward but always becomes blunter. Thus, this minimal model of crack-like failure appears initially to be ductile.

The results in [1] tell us that this oversimplified picture must change dramatically when we include the time dependent variation of the effective disorder temperature near the crack tip. If the initial effective temperature is small, then the stress-induced deformation creates an effective hot spot at the tip, which generates new STZ’s there, and launches a sharp crack in agreement with the observations in [2]. My purpose here is to predict when and how this happens.

The mathematical elements of this analysis are contained in Secs. II, III, and IV; and the numerical results are presented in Sec.V. Section VI contains concluding remarks.

## II. ELLIPTICAL CRACK: PRELIMINARY REMARKS

Consider an incompressible plate of elasto-plastic material lying in the  $x, y$  plane and containing an elliptical hole. The ellipse is elongated in the  $x$  direction; and a mode-I stress  $\sigma_\infty$  is imposed in the  $y$  direction very

far from the hole. Assume hypo-elasto-plasticity (additive decomposition of elastic and plastic rates of deformation) and, in the first stage of the analysis, assume the simplest possible Bingham plasticity law with a fixed yield stress and a fixed ratio between deformation rate and incremental stress above yield. (See Eq.(3.2) below.)

The static, linearly elastic version of this problem has been solved by Muskhelishvili [10]. The first step is to transform from Cartesian coordinates  $(x, y)$  to elliptical coordinates  $(\rho, \theta)$ :

$$x = W \left( \rho + \frac{m}{\rho} \right) \cos \theta, \quad y = W \left( \rho + \frac{m}{\rho} \right) \sin \theta. \quad (2.1)$$

Curves of constant  $\rho$  are ellipses, and curves of constant  $\theta$  are orthogonal hyperbolas. If we take the boundary of the elliptical hole to be at  $\rho = 1$ , then the semi-major and semi-minor axes of the ellipse have lengths  $W(1+m)$  and  $W(1-m)$  respectively. Let  $0 < m < 1$  so that the long axis of the ellipse lies in the  $x$  direction, perpendicular to the applied stress, in analogy to a mode-I crack.

To produce a long, thin ellipse, let  $W$  become larger than any other length in the system, and fix  $m \leq 1$  so that the curvature at the tip, i.e. at  $x = W(1+m)$ , is large but finite. Denote this curvature by  $\mathcal{K}_{tip}$ . Then a calculation to leading order in  $1/\sqrt{W}$  yields

$$m \approx 1 - 2\epsilon; \quad \epsilon \equiv \sqrt{\frac{1}{2\mathcal{K}_{tip}W}} \ll 1, \quad (2.2)$$

where  $\epsilon$  will be the principal small parameter in this analysis.

My scheme is to try to use the elasto-plastic equations of motion to determine the behavior of this elliptical crack tip under simple forcings. There are two serious difficulties with this scheme. First, we know that this shape does not remain elliptical; its irreversible motion must involve shape changes that cannot be described simply by time dependent values of the elliptical tip parameters  $W$  and  $\mathcal{K}_{tip}$ . Second, we know that the coupled elastic and plastic deformations become spatially complex in more than one dimension. Irreversible plastic deformation in the neighborhood of the crack tip substantially modifies the stress field at the crack surface in a way that is not easily described analytically with any generality.

About a decade ago, my colleagues and I [11] addressed both of these difficulties by considering STZ elasto-plasticity in the neighborhood of an expanding circular hole, where variations in the geometry of the hole and in the neighboring elasto-plastic fields occur only in the radial direction. Our stated motivation was to gain some insight regarding the fracture problem. We did test a boundary-layer approximation similar to the one that I shall use here; but the circular symmetry was inconsistent with the stress concentration at a sharp tip that is needed to describe fracture. (Ref. [11] was motivated in part by my earlier paper [12] in which I introduced the elliptical model used here. Unfortunately, [12] is incorrect;

both its mathematical analysis and its main conclusions are wrong.)

To minimize the difficulties of the elliptical approximation, I focus only on the immediate neighborhood of the sharp tip and look only at the early onset of plastic deformation there. I rely heavily on dimensional analysis. Also, to simplify the presentation, I have relegated the general elliptical formulas to the Appendix, and use only near-tip and early-onset approximations derived from those formulas in the main text.

### III. ELLIPTICAL CRACK: BINGHAM ELASTOPLASTICITY

Start with the rate-of-plastic-deformation tensor for an incompressible sheet. The diagonal elements of this tensor are:

$$D_{\theta\theta}^{pl} = -D_{\rho\rho}^{pl} \equiv D^{pl}, \quad (3.1)$$

where, initially, I assume a simple Bingham law with a yield stress  $s_y$  and a constant plastic rate factor  $1/\tau_{pl}$ :

$$D^{pl}(\rho, \theta) = \frac{1}{\tau_{pl}} \left[ \left[ \frac{s(\rho, \theta)}{s_y} - 1 \right] \right]. \quad (3.2)$$

Here,  $s(\rho, \theta) \equiv s_{\theta\theta}(\rho, \theta) = -s_{\rho\rho}(\rho, \theta)$  are the diagonal elements of the deviatoric stress, which I assume to be non-negative for present purposes.

In Eq.(3.2), I have used a notation that will be convenient in much of what follows. The double brackets mean that  $[[f]] = f$  if  $f \geq 0$  and  $[[f]] = 0$  otherwise.

Eq.(A6) in the Appendix can be used to derive an expression for the deviatoric stress  $s(\rho, \theta)$  near the elliptical tip, in the absence of plasticity. Let  $\rho = 1 + \tilde{x}$ , with  $\tilde{x} \ll 1$ , and use the definition of  $\epsilon$  in Eq.(2.2). I find:

$$s(\rho, \theta) \equiv \tilde{s}(\tilde{x}, \theta) \cong \frac{\sigma_\infty \epsilon^2}{(\epsilon + \tilde{x})^3} \left( 1 - \frac{2\theta^2}{\epsilon^2} \right). \quad (3.3)$$

Next, note that for  $\tilde{x} = 0$  and  $\theta = 0$ , Eq.(3.3) can be written

$$\frac{\tilde{s}(0, 0)}{s_y} = \frac{\sigma_\infty}{s_y \epsilon} \equiv \psi \sqrt{\kappa}, \quad (3.4)$$

where

$$\psi \equiv \frac{\sigma_\infty}{s_y} \sqrt{\frac{2W}{a}}; \quad \kappa \equiv a \mathcal{K}_{tip}, \quad (3.5)$$

and  $a$  is a fixed length scale of the order of magnitude of the initial tip radius that I have chosen for dimensional convenience. (It plays no quantitative role in the physics.) Thus,  $\psi$  is a dimensionless measure of the stress intensity factor, where the small applied stress  $\sigma_\infty$  is amplified by the large factor  $\sqrt{W/a}$ .

At this point in the development, we must pay attention to the plastic zone that forms near the tip when the

stress given by Eq.(3.3) exceeds  $s_y$  at some nonzero value of  $\tilde{x}$ , say  $\tilde{x}_{max}$ . For  $\theta = 0$ ,

$$\tilde{x}_{max} = \epsilon [[\nu - 1]], \text{ where } \nu \equiv \left(\frac{\sigma_\infty}{\epsilon s_y}\right)^{1/3} = (\psi\sqrt{\kappa})^{1/3}. \quad (3.6)$$

The onset of plastic deformation at the tip occurs when  $\nu = 1$ ; that is, when  $\psi = \kappa^{-1/2}$ .

It is important to understand the significance of the quantity  $[[\nu - 1]]$ . According to Eq.(2.1), the position of the tip on the  $x$  axis is

$$x_0 = W(1 + m) \cong 2W(1 - \epsilon), \quad (3.7)$$

and the front edge of the plastic zone is at

$$\begin{aligned} x_{max} &= W \left(1 + \tilde{x}_{max} + \frac{1 - 2\epsilon}{1 + \tilde{x}_{max}}\right) \\ &\cong x_0 + \frac{1}{\mathcal{K}_{tip}} [[\nu - 1]]. \end{aligned} \quad (3.8)$$

Thus,  $[[\nu - 1]] = \mathcal{K}_{tip}(x_{max} - x_0)$  is the thickness of the plastic zone in units of the radius of curvature at the tip, which must be of order unity or smaller in order to validate the boundary-layer approximation.

In the absence of an exact solution for the stress field inside the plastic zone, analogous to that found in [11], I propose the following boundary-layer approximation for Eq.(3.2):

$$D^{pl}(\rho, \theta) \cong \tilde{D}^{pl}(\tilde{x}, \theta) = \frac{1}{\tau_{pl}} \left[ \frac{\tilde{s}(\tilde{x}, 0)}{s_y} - 1 \right] \left(1 - \frac{2\theta^2}{\epsilon^2}\right) \quad (3.9)$$

where

$$\frac{\tilde{s}(\tilde{x}, 0)}{s_y} - 1 \cong \left(\frac{s_0}{s_y} - 1\right) \left(1 - \frac{\tilde{x}}{\tilde{x}_{max}}\right). \quad (3.10)$$

That is,  $\tilde{s}(\tilde{x}, 0)$  is approximated by a linear function of  $\tilde{x}$  across the boundary layer; and  $s_0 = \tilde{s}(0, 0)$  is a boundary stress yet to be determined. This kind of approximation worked well in [11]; I shall use it throughout this paper.

We now can use Eqs.(A1) and (A2) in the Appendix to compute the rate of deformation tensor in terms of the material velocities  $v_\rho^{pl}$  and  $v_\theta^{pl}$  near the crack tip. Using the same approximations for small  $\tilde{x}$  and small  $\theta$  used above, I find

$$D_{\rho\rho}^{pl} \approx \frac{1}{2\epsilon W} \left[ \frac{\partial v_\rho^{pl}}{\partial \tilde{x}} + \frac{\partial v_\theta^{pl}(0)}{\partial \theta} \frac{\theta^2}{\epsilon^2} \right] \left(1 - \frac{\theta^2}{2\epsilon^2}\right); \quad (3.11)$$

and

$$D_{\theta\theta}^{pl} \approx \frac{1}{2\epsilon W} \left[ \frac{\partial v_\theta^{pl}}{\partial \theta} + \frac{v_\rho^{pl}}{\epsilon} \left(1 - \frac{\theta^2}{\epsilon^2}\right) \right] \left(1 - \frac{\theta^2}{2\epsilon^2}\right). \quad (3.12)$$

Then, setting  $\theta = 0$  in Eq.(3.11), and using Eqs.(3.1) and (3.2), compute the plastic part of the tip velocity:

$$v_{tip}^{pl} = - \int_0^{\tilde{x}_{max}} \frac{dv_\rho^{pl}}{d\tilde{x}} d\tilde{x}$$

$$\begin{aligned} &= \frac{2\epsilon W}{\tau_{pl}} \left(\frac{s_0}{s_y} - 1\right) \int_0^{\tilde{x}_{max}} d\tilde{x} \left(1 - \frac{x}{\tilde{x}_{max}}\right) \\ &= \frac{\epsilon W}{\tau_{pl}} \left(\frac{s_0}{s_y} - 1\right) [[\tilde{x}_{max}]] \\ &= \frac{a}{2\kappa \tau_{pl}} \left(\frac{s_0}{s_y} - 1\right) [[\nu(\psi, \kappa) - 1]]. \end{aligned} \quad (3.13)$$

Finally, because the quantity  $s_0/s_y - 1$  vanishes at the onset of plasticity, it should be proportional to  $\tilde{x}_{max} \propto [[\nu - 1]]$ ; and we can resolve the  $s_0$  uncertainty by assuming that

$$\frac{s_0}{s_y} - 1 \propto [[\nu(\psi, \kappa) - 1]] \quad (3.14)$$

and by absorbing the dimensionless proportionality factor into the rate factor  $1/\tau_{pl}$ . Thus,

$$v_{tip}^{pl} \cong \frac{a}{2\kappa \tau_{pl}} [[\nu(\psi, \kappa) - 1]]^2. \quad (3.15)$$

Now use this boundary-layer approximation to derive an equation of motion for the radius of curvature at the tip. Start with the geometric formula

$$-\frac{\dot{\mathcal{K}}_{tip}^{pl}}{\mathcal{K}_{tip}^2} = v_{tip}^{pl} + \frac{1}{2\mathcal{K}_{tip}W} \frac{\partial^2 v_\rho^{pl}}{\partial \theta^2} \Big|_{\theta=0}. \quad (3.16)$$

Use Eq.(3.12) at  $\theta = 0$  to find

$$\begin{aligned} \frac{\partial v_\theta^{pl}}{\partial \theta}(\theta = 0) &= -\frac{v_{tip}^{pl}}{\epsilon} + \frac{2\epsilon W}{\tau_{pl}} \left(\frac{s_0}{s_y} - 1\right) \\ &= \frac{2\epsilon W}{\tau_{pl}} \left(\frac{s_0}{s_y} - 1\right)(3 - \nu). \end{aligned} \quad (3.17)$$

Then write Eq.(3.11) in the form

$$v_\rho^{pl}(\tilde{x} = 0) = - \int_0^{\tilde{x}_{max}} d\tilde{x} \frac{\partial v_\rho^{pl}}{d\tilde{x}} = v_{tip}^{pl} + \frac{\theta^2}{\epsilon^2} A, \quad (3.18)$$

where, with Eq.(3.17),

$$A \cong \frac{\epsilon^2 W}{2\tau_{pl}} \left(\frac{s_0}{s_y} - 1\right)(\nu - 1). \quad (3.19)$$

Finally, combining Eqs.(3.14), (3.15), (3.16), and (3.18), and using the  $\kappa$  notation introduced in Eq.(3.5), we obtain

$$\dot{\kappa}^{pl} = -\frac{\kappa}{\tau_{pl}} [[\nu(\psi, \kappa) - 1]]^2. \quad (3.20)$$

The minus sign implies – remarkably – that the tip always blunts at the onset of plastic deformation in this model.

It remains to include the elastic driving force in these calculations. The elastic displacement field given in Eq.(A9), at a sharp tip, reduces simply to

$$u_\rho^{el} + iu_\theta^{el} \approx -\frac{W\sigma_\infty}{2\mu} \left(1 - \frac{i\theta}{\epsilon} - \frac{\theta^2}{2\epsilon^2}\right). \quad (3.21)$$

Set  $\theta = 0$  and take a time derivative to find

$$\begin{aligned} v_{tip}^{el} &= -\frac{1}{2\mu} \frac{d}{dt} (W\sigma_\infty) = -\frac{1}{2\mu} \frac{d}{dt} \left( s_y \psi \sqrt{\frac{aW}{2}} \right) \\ &= -\frac{s_y}{2\mu} \sqrt{\frac{aW}{2}} \left( \dot{\psi} + \frac{\dot{W}}{2W} \psi \right) \end{aligned} \quad (3.22)$$

The last term proportional to  $\dot{W}/W$  is negligible for large  $W$ . Thus we can write the total tip velocity in the form

$$\frac{v_{tip}}{a} = \frac{v_{tip}^{pl}}{a} - \frac{s_y}{2\mu} \sqrt{\frac{W}{2a}} \dot{\psi}. \quad (3.23)$$

Following [13], identify  $\dot{\psi}$  as the external driving rate  $\tau_{ex}^{-1}$ , and define

$$\xi \equiv \frac{\tau_{ex}}{\tau_{pl}}; \quad \tau_{ex} \frac{d}{dt} \equiv \frac{d}{d\psi}. \quad (3.24)$$

Then Eq.(3.23) becomes

$$\tilde{v}_{tip}(\psi, \kappa) \equiv \frac{v_{tip} \tau_{ex}}{a} = \frac{\xi}{2\kappa} [[\nu(\psi, \kappa) - 1]]^2 - c_0, \quad (3.25)$$

where

$$c_0 = \frac{s_y}{2\mu} \sqrt{\frac{W}{2a}} \quad (3.26)$$

is a system-specific dimensionless constant. Alternatively, define a dimensionless tip displacement  $\tilde{u}_{tip}(\psi, \kappa)$  so that Eq.(3.25) becomes

$$\frac{d\tilde{u}_{tip}}{d\psi} = \frac{\xi}{2\kappa} [[\nu(\psi, \kappa) - 1]]^2 - c_0, \quad (3.27)$$

A similar analysis using the  $\theta^2$  term in Eq.(3.21) and the geometric formula in Eq.(3.16) (for the additive elastic part of the rate of deformation) yields

$$\dot{\kappa}^{el} = -2c_0\kappa^2; \quad (3.28)$$

and thus, adding elastic and plastic parts,

$$\frac{d\kappa}{d\psi} = -\xi \kappa [[\nu(\psi, \kappa) - 1]]^2 - 2c_0\kappa^2. \quad (3.29)$$

#### IV. EFFECTIVE TEMPERATURE DYNAMICS

To make contact with the Ref.[1] simulations, we must introduce the space and time dependent effective temperature  $\chi$  that determines the local density of flow defects, that is, STZ's. The basic assumption is that the plastic deformation rate is proportional to this density which, in turn, is proportional to an effective thermal activation factor. I write this modified rate factor in the form:

$$\frac{1}{\tau_{pl}} e^{-e_Z/\chi(\theta,t)} e^{e_Z/\chi_\infty} \quad (4.1)$$

where  $e_Z$  is the STZ formation energy. The first factor,  $1/\tau_{pl}$ , is the same as the one introduced in Eq.(3.2) to describe simple Bingham plasticity. The second is the STZ activation factor, and the last term adjusts that factor so that, in the steady-state limit,  $\chi \rightarrow \chi_\infty$ , and we recover the Bingham result.

The effective temperature  $\chi$  needs to be evaluated here only on the surface of the crack tip. Thus, I modify Eq.(3.9) to read

$$\begin{aligned} \tilde{D}^{pl}(\tilde{x}, \theta) &= \frac{1}{\tau_{pl}} e^{-e_Z/\chi(\theta,t)} e^{e_Z/\chi_\infty} \\ &\times \left( \frac{s_0}{s_y} - 1 \right) \left[ \left[ 1 - \frac{\tilde{x}}{\tilde{x}_{max}} \right] \right] \left( 1 - \frac{2\theta^2}{\epsilon^2} \right). \end{aligned} \quad (4.2)$$

Let

$$\chi(\theta, t) = \chi(t) - \gamma(t) \frac{\theta^2}{\epsilon^2}; \quad \gamma(t) = -\frac{\epsilon^2}{2} \frac{\partial^2 \chi}{\partial \theta^2} \Big|_{\theta=0}, \quad (4.3)$$

and  $\chi(t) \equiv \chi(\theta = 0, t)$ . Then

$$e^{-e_Z/\chi(\theta,t)} \cong e^{-e_Z/\chi(t)} \left( 1 - \frac{e_Z \gamma(t) \theta^2}{\chi^2(t) \epsilon^2} \right); \quad (4.4)$$

and

$$\begin{aligned} \tilde{D}^{pl}(\tilde{x}, \theta) &\cong \frac{1}{\tau_{pl}} e^{-e_Z/\chi(t)} e^{e_Z/\chi_\infty} \left( \frac{s_0}{s_y} - 1 \right) \\ &\times \left[ \left[ 1 - \frac{\tilde{x}}{\tilde{x}_{max}} \right] \right] \left[ 1 - \frac{\theta^2}{\epsilon^2} \left( 2 + \frac{e_Z \gamma(t)}{\chi^2(t)} \right) \right]. \end{aligned} \quad (4.5)$$

We next need equations of motion for  $\chi(t)$  and  $\gamma(t)$ . The basic equation of motion for  $\chi(\theta, t)$  has the form

$$c_{eff} \dot{\chi}(\theta, t) = \tilde{D}^{pl}(0, \theta) \tilde{s}(0, \theta) \left[ 1 - \frac{\chi(\theta, t)}{\chi_\infty} \right]. \quad (4.6)$$

This is the effective heat-flow equation that has been conventional in STZ theory.  $c_{eff}$  is the effective specific heat; the product  $\tilde{D}^{pl} \tilde{s}$  is the rate at which power is delivered to the tip region by the plastic deformation; and  $\chi_\infty$  is the steady-state value of  $\chi$ . Eq.(4.5) tells us what to use for  $\tilde{D}^{pl}(0, \theta)$  here; and  $\tilde{s}(0, \theta) \approx s_y(1 - 2\theta^2/\epsilon^2)$  is accurate enough for this purpose. Inserting these ingredients into Eq.(4.6) and setting  $\theta = 0$ , we find

$$c_{eff} \dot{\chi} = \frac{1}{\tau_{pl}} e^{-e_Z/\chi} e^{e_Z/\chi_\infty} s_y \left( \frac{s_0}{s_y} - 1 \right) \left( 1 - \frac{\chi}{\chi_\infty} \right). \quad (4.7)$$

Then, by equating coefficients of  $\theta^2$  in Eq.(4.6), we obtain an equation of motion for the new angular variable  $\gamma(t)$ :

$$\begin{aligned} c_{eff} \dot{\gamma} &= \frac{1}{\tau_{pl}} \left( \frac{s_0}{s_y} - 1 \right) e^{-e_Z/\chi} e^{e_Z/\chi_\infty} \\ &\times \left[ 4 \left( 1 - \frac{\chi}{\chi_\infty} \right) + \left( \left( 1 - \frac{\chi}{\chi_\infty} \right) \frac{e_Z}{\chi^2} - \frac{1}{\chi_\infty} \right) \gamma \right]. \end{aligned} \quad (4.8)$$

As in earlier papers, it is convenient to introduce the notation  $\tilde{\chi} = \chi/e_Z$  and, similarly,  $\tilde{\gamma} = \gamma/e_Z$ . Making this substitution, and using Eq.(3.14) to evaluate the factors containing  $s_0$ , we find the following:

$$\frac{d\tilde{u}_{tip}}{d\psi} = \tilde{v}_{tip} = \xi \frac{e^{-1/\tilde{\chi}+1/\tilde{\chi}_\infty}}{2\kappa} [[\nu(\psi, \kappa) - 1]]^2 - c_0, \quad (4.9)$$

where  $\tilde{v}_{tip}(\psi, \kappa, \tilde{\chi}) \equiv v_{tip} \tau_{ex}/a$ , and  $\xi \equiv \tau_{ex}/\tau_{pl}$  as before. The curvature equation becomes

$$\frac{d\kappa}{d\psi} = -\xi \kappa e^{-1/\tilde{\chi}+1/\tilde{\chi}_\infty} [[\nu(\psi, \kappa) - 1]]^2 \left(1 - \frac{2\tilde{\gamma}}{\tilde{\chi}^2}\right) - 2c_0 \kappa^2. \quad (4.10)$$

Note that the term proportional to  $\tilde{\gamma}$  in this equation, when large enough, produces tip sharpening.

The equation of motion for  $\tilde{\chi}$ , Eq.(4.7), becomes

$$\frac{d\tilde{\chi}}{d\psi} = c_1 \xi e^{-1/\tilde{\chi}+1/\tilde{\chi}_\infty} [[\nu(\psi, \kappa) - 1]] \left(1 - \frac{\tilde{\chi}}{\tilde{\chi}_\infty}\right), \quad (4.11)$$

where  $c_1 = (s_y/e_Z c_{eff})$  is a dimensionless prefactor. Finally, the equation of motion for  $\tilde{\gamma}$ , Eq.(4.8), becomes

$$\begin{aligned} \frac{d\tilde{\gamma}}{d\psi} &= c_1 \xi e^{-1/\tilde{\chi}+1/\tilde{\chi}_\infty} [[\nu(\psi, \kappa) - 1]] \\ &\times \left[ 4\left(1 - \frac{\tilde{\chi}}{\tilde{\chi}_\infty}\right) + \left(1 - \frac{\tilde{\chi}}{\tilde{\chi}_\infty}\right) \frac{1}{\tilde{\chi}^2} - \frac{1}{\tilde{\chi}_\infty} \right] \tilde{\gamma}. \end{aligned} \quad (4.12)$$

## V. NUMERICAL RESULTS

To evaluate the formulas in Secs.III and IV, we need values for a small number of physical parameters. My main goal is to make contact with the experimental data of Ref. [2], especially with the measurements of fracture toughness for the metallic glass Vitreloy 1 (Zr<sub>41.2</sub>Ti<sub>13.8</sub>Cu<sub>12.5</sub>Ni<sub>10</sub>Be<sub>22.5</sub>). I am able to do that in a limited but nontrivial way.

From [2], I find that the notch depth is  $W \sim 2.5 \times 10^{-3}$  m, and  $a \sim 10^{-5}$  m is roughly the initial tip radius. I also know from [1] and other sources that  $\mu \sim 40$  GPa and  $s_y \sim 1$  GPa. Thus, in Eq.(3.26), I estimate  $c_0 \sim 0.1$ . To determine  $c_1$  in Eqs.(4.11) and (4.12), however, I would need an estimate of the effective specific heat  $c_{eff}$ . Without such an estimate, Rycroft and Bouchbinder [1] seem to have used simply  $c_1 = 1$ ; and I shall do the same.

In Refs. [14] and [15], I looked critically at the STZ-theoretical description of yielding in amorphous systems, and used the experimental data for Vitreloy 1 by Lu et al. [16] as the basis for my analysis. I found there that  $e_Z/k_B \cong 960$  K and that  $\tilde{\chi}_\infty \cong 0.2$ . I use this estimate in the effective-temperature analyses described below. However, I have not tried to evaluate the rate-ratio  $\xi$  from first principles (e.g. from the analysis in [14]). That uncertainty, and – more importantly – my fundamental inability to compute measured fracture toughnesses, means that I can achieve only semi-quantitative agreement with the toughness data in [2].

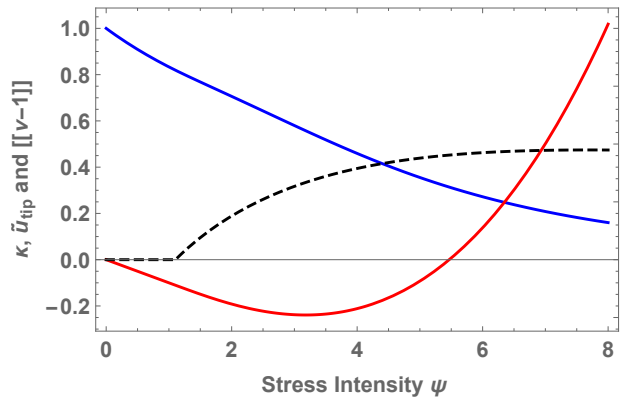


FIG. 1: Dimensionless tip curvature  $\kappa$  (top, blue), tip displacement  $\tilde{u}_{tip}$  (bottom, red), and relative boundary-layer thickness  $[[\nu - 1]]$  (black, dashed) as functions of the dimensionless stress intensity  $\psi$ , for rate-ratio  $\xi = 1$ .

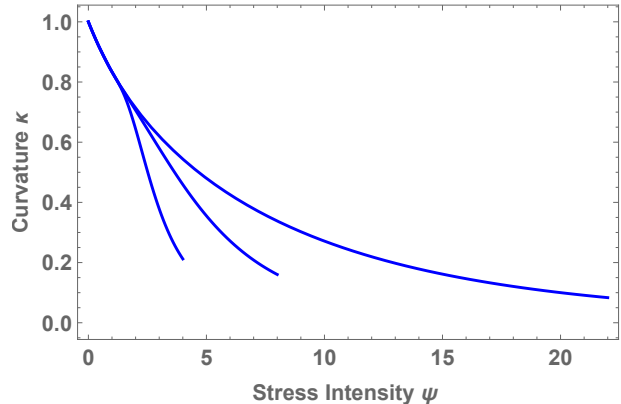


FIG. 2: Dimensionless tip curvatures  $\kappa$  as functions of dimensionless stress intensity  $\psi$ , for rate-ratios  $\xi = 10, 1,$  and  $0.1,$  from left to right.

Figure 1 is a partial summary of the Bingham results obtained by solving the equations derived in Sec.III. All of the curves shown in this figure are for  $\xi = 1$ . The top curve (blue) is the dimensionless tip curvature  $\kappa(\psi)$ , the solution of Eq.(3.29). It is a monotonically decreasing function, illustrating the fact that this model predicts only tip blunting. The bottom curve (red) is the tip displacement  $\tilde{u}_{tip}$ , determined by solving Eq.(3.27). Note that this displacement is initially negative, governed by the elastic forcing, and does not start to rise again until well after the onset of plasticity near  $\psi = 1$ . The tip regains its initial position,  $\tilde{u}_{tip} = 0$ , at  $\psi \equiv \psi_c \cong 5.5$ , which I propose to be a physically well-defined measure of the early-stage fracture toughness for this ductile situation. The dashed (black) curve in Fig.1 is  $[[\nu - 1]]$ , the ratio of the thickness of the plastic boundary layer to

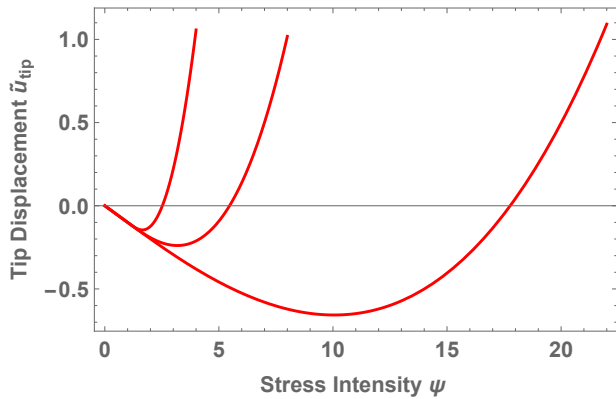


FIG. 3: Dimensionless tip displacements  $\tilde{u}_{tip}$  as functions of dimensionless stress intensity  $\psi$ , for rate-ratios  $\xi = 10, 1$ , and  $0.1$ , from left to right.

the tip radius, which is seen to remain safely below unity throughout this process.

Figures 2 and 3 tell us more about the dynamics of the Bingham model by showing how the tip curvature  $\kappa$  and the tip displacement  $\tilde{u}_{tip}$ , respectively, change their behaviors as we decrease the rate-ratio  $\xi$  from 10 to 0.1. Note especially in Fig.3 that my nominal fracture toughness  $\psi_c$  increases from about 3 to 5.5 to about 18 with this sequence of exponentially decreasing values of  $\xi$ . For this purely ductile Bingham model, decreasing  $\xi$  might correspond to decreasing the ordinary temperature and, thus, increasing toughness. These results seem plausible although they look, at first, to be the opposite of those described in [13].

Turn now to the predictions of the effective-temperature theory presented in Sec. IV. In the following, I present solutions of Eqs.(4.9 - 4.12) for a fixed value of the rate-ratio,  $\xi = 1$ , for  $\tilde{\chi}_\infty = 0.20$ , and for a sequence of five decreasing initial values of the effective temperature  $\tilde{\chi}_0 = 0.160, 0.150, 0.145, 0.140$ , and  $0.135$ . These dimensionless effective temperatures correspond to fictive temperatures of  $770\text{ K}, 720\text{ K}, 696\text{ K}, 672\text{ K}$ , and  $648\text{ K}$ , which may be somewhat above the range of temperatures in which the brittle-ductile transition occurs according to [2]. They could easily be adjusted downward by adjusting the value of  $\xi$  or  $e_Z/k_B$ .

The most remarkable observation of [1] is that the sharpening of the crack tip generated by the local increase in effective temperature produces a negative-pressure spike ahead of the tip, and that this pressure spike can be strong enough to cause cavitation and thus launch a new crack segment. All of this happens much too quickly to be described by the present quasi-static theory. Of course, cavitation would not actually occur in this theory of incompressible elasticity. Nevertheless, the theory is accurate enough to predict the pressure spike and, thus, the onset of some new kind of presumably

brittle behavior.

The pressure near the elliptical hole is given by one half of the right-hand side of Eq.(A5). Evaluating this expression at the outer edge of the plastic zone ahead of the crack tip, i.e. at  $\tilde{x}_{max}$ , I find:

$$\frac{p_{tip}}{s_y} \approx -\nu^2 = -(\psi\sqrt{\kappa})^{2/3}. \quad (5.1)$$

In [1], it is estimated that the critical pressure for cavitation is  $p_c/s_y \cong -5$ .

The pressure, as a function of the stress intensity  $\psi$ , is included in Fig. 4. This figure is analogous to the Bingham case shown in Fig.1. Here I have used a reduced value of  $\tilde{\chi}_0 = 0.15 < \tilde{\chi}_\infty$  so that we can see the early effects of the initially decreased effective temperature. The tip sharpens briefly but relaxes and flattens again as the enhanced effective-temperature field in its neighborhood spreads out and approaches its steady-state value. The pressure does not quite reach the critical value for cavitation. Predicting the subsequent motion of the crack is well beyond the limitations of the present theory. Without being able to compute the non-elliptic deformation of the crack tip and its associated growing plastic zone, I cannot predict the result of a conventional measurement of fracture toughness.

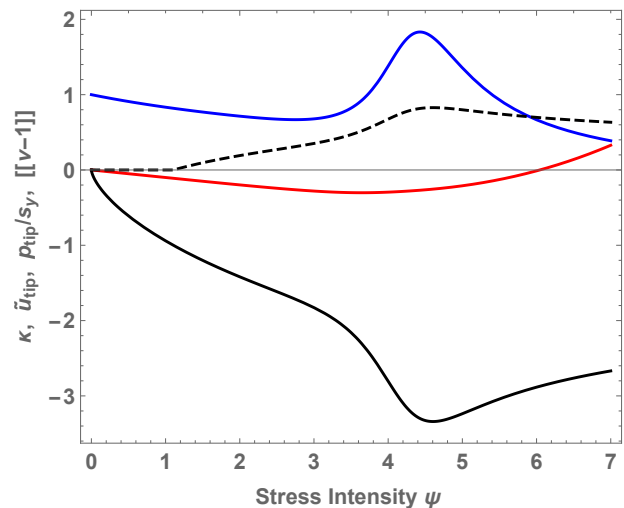


FIG. 4: Dimensionless tip curvature  $\kappa$  (top, blue), tip displacement  $\tilde{u}_{tip}$  (middle, red), relative boundary-layer thickness  $[(\nu - 1)]$  (black, dashed), and pressure ahead of the tip  $p_{tip}/s_y$  (bottom, black) as functions of the dimensionless stress intensity  $\psi$ , for rate-ratio  $\xi = 1$ ,  $\tilde{\chi}_\infty = 0.20$ , and dimensionless effective temperature  $\tilde{\chi}_0 = 0.15$ .

Figures 5 and 6 show that the tip undergoes a runaway sharpening instability at a stress intensity of  $\psi \cong 4.5$  for values of  $\tilde{\chi}_0 \leq 0.14$  (i.e. below about  $670\text{ K}$ , in approximate agreement with the experiments). This is seen both in the curvature curves in Fig. 5 and the pressure curves in Fig. 6. The pressure reaches its cavitation threshold,

## VI. REMARKS

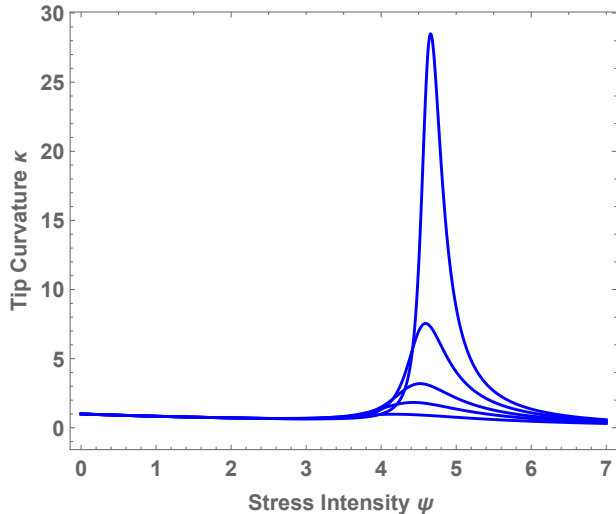


FIG. 5: Dimensionless tip curvatures  $\kappa$  as functions of the dimensionless stress intensity  $\psi$ , for rate-ratio  $\xi = 1$ ,  $\tilde{\chi}_\infty = 0.20$ , and initial dimensionless effective temperatures  $\tilde{\chi}_0 = 0.160, 0.150, 0.145, 0.140, 0.135$  from bottom to top.

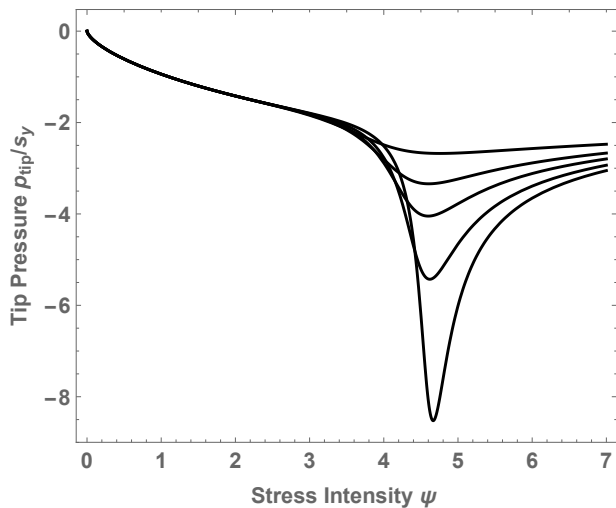


FIG. 6: Pressures  $p_{tip}/s_y$  ahead of the crack tip as functions of the dimensionless stress intensity  $\psi$ , for rate-ratio  $\xi = 1$ ,  $\tilde{\chi}_\infty = 0.20$ , and initial dimensionless effective temperatures  $\tilde{\chi}_0 = 0.160, 0.150, 0.145, 0.140, 0.135$  from top to bottom.

$p_c/s_y \sim -5$ , also for  $\tilde{\chi}_0 \leq 0.14$ . In both figures, I am pushing the theory well beyond its limits of validity by extending the curves up to and beyond their peaks. But these parts of the curves are not to be taken literally. I think that the main conclusion is correct – that there is a qualitative transition between ductile and brittle behaviors at this instability.

I have long been skeptical about various aspects of conventional materials science, especially dislocation theory (e.g. see [8]), because results often are based on non-predictive phenomenology. The results presented here make me more optimistic about opportunities for improving the situation. But there are many open issues.

*Yielding Transitions.* A key assumption throughout this analysis is that the yielding transition is sharp and nonsingular, *i.e.* that it is Bingham-like near threshold. This is not true in many rheological models, for example, in Herschel-Bulkley models where the flow rate is proportional to the square root of the incremental stress above the yield stress  $s_y$ . There is also the possibility that yielding transitions may be critical phenomena accompanied by diverging fluctuations. That is what happens in athermal quasistatic models which ignore the fact that internal relaxation rates necessarily become much faster than external driving rates when the latter vanish at a yield point.

My papers [14] and [15] were written in large part to explore the nature of yielding transitions in STZ theories of amorphous materials, especially metallic glasses. In [15], I argued from first principles that realistic yielding transitions of this kind are non-critical. I also showed in [15] that the Bingham model can be derived as a limit of STZ theory.

*Dislocations.* One of my original motives for starting this project was the idea that the new thermodynamic dislocation theory [6–8] must be relevant to fracture toughness. The problem of understanding brittleness and ductility in metals and alloys and other crystalline materials is far more complex than it is for amorphous materials. Just the existence of grain boundaries makes this topic seem formidable. Nevertheless, important progress has been made in the last decade simply by realizing that dislocations in driven systems must obey the second law of thermodynamics and thus must be amenable to an effective-temperature analysis. That realization has led to successful first-principles theories of strain hardening and sharp yielding transitions, both of which are relevant to fracture.

The picture developed here of brittle fracture being initiated in a metallic glass at a low fictive temperature looks almost identical to the picture of a notch in an unhardened crystalline material with a low initial density of dislocations. The external stress generates dislocations at an effectively hot spot at the tip of the notch. It should be possible to use the new dislocation theory to predict how rapidly that happens and what happens next. There are many such opportunities for progress along these lines.

*Fracture Dynamics.* This theory of the onset of brittle or ductile fracture occupies just a tiny corner of the large field of fracture dynamics. As I have emphasized at various places in this paper, it is not obvious how to bridge the gap between this corner and the rest of the field.

Note that my equations of motion in Secs. III and IV do not look like those that appear in the conventional literature on fracture dynamics. In the conventional picture (e.g. see Freund [17]), we visualize a Griffiths-like crack moving on a well defined plane, driven by remote loading that causes elastic energy to flow to the crack tip, where that energy is somehow dissipated. For many years, the most promising descriptions of the tip behavior seemed to be the cohesive-zone models of Dugdale and Barenblatt.[18, 19] Sometimes those cohesive zones were called “plastic” zones; but the models never included realistic equations of motion for the plastic flow fields  $v_\rho^{pl}$  and  $v_\theta^{pl}$  that appear here. Moreover, it has been known for twenty years that most cohesive-zone models are intrinsically ill-posed; they produce strongly unstable cracks if they describe cracks at all.[20, 21]

In my opinion, some of the most interesting recent developments in fracture dynamics are those described by Bouchbinder and colleagues in Refs.[22–24]. These authors develop nonlinear field theories to describe the dynamics of fast cracks, and show that their theories predict high-speed behaviors, including instabilities and sidebranching, in agreement with experimental observations. Those theories are not – and cannot be – simple extensions of the quasistatic onset behavior studied here. Both of these related but qualitatively different classes of behavior – the onset behavior that determines brittleness and ductility, the late-stage behavior that determines large-scale failure, and the range of phenomena that lies between them – continue to be highly promising areas for research.

### Appendix A: Elliptical Formulas

For completeness, I list in this Appendix the formulas on which I have based my analyses. The elliptical coordinates are defined in Eq.(2.1).

First, there are expressions for the rate-of-deformation tensor  $D$  in terms of the elliptical material velocity components  $v_\rho$  and  $v_\theta$  as derived from more general formulas in Malvern [25].

$$D_{\rho\rho} = \frac{1}{WN} \left[ \frac{\partial v_\rho}{\partial \rho} + \frac{v_\theta}{\rho} \frac{1}{N} \frac{\partial N}{\partial \theta} \right]; \quad (\text{A1})$$

$$D_{\theta\theta} = \frac{1}{WN\rho} \left[ \frac{\partial v_\theta}{\partial \theta} + \frac{v_\rho}{N} \frac{\partial}{\partial \rho}(\rho N) \right]; \quad (\text{A2})$$

and

$$D_{\rho\theta} = \frac{1}{2WN} \left[ \frac{1}{\rho} \frac{\partial v_\rho}{\partial \theta} + \frac{\partial v_\theta}{\partial \rho} - \frac{v_\rho}{N\rho} \frac{\partial N}{\partial \theta} - \frac{v_\theta}{N\rho} \frac{\partial(N\rho)}{\partial \rho} \right]; \quad (\text{A3})$$

where the metric function is

$$N^2(\rho, \theta) = 1 + \frac{m^2}{\rho^4} - \frac{2m}{\rho^2} \cos 2\theta. \quad (\text{A4})$$

Then there are the formulas for incompressible, two-dimensional elasticity that I have derived from Muskhelishvili [10]. The following formulas assume vanishing

normal stress on the surface of the elliptical hole, that is, at  $\rho = 1$ . The stress tensor  $\sigma$  is given by

$$\sigma_{\rho\rho} + \sigma_{\theta\theta} = \sigma_\infty \text{Re} \left[ 1 + \frac{2(1+m)e^{-2i\theta}}{\rho^2 - m e^{-2i\theta}} \right]; \quad (\text{A5})$$

and

$$\begin{aligned} \mathcal{S}(\rho, \theta) &\equiv \sigma_{\theta\theta} - \sigma_{\rho\rho} + 2i\sigma_{\rho\theta} \\ &= \frac{\sigma_\infty \rho^2 e^{2i\theta}}{(\rho^2 - m e^{2i\theta})} \\ &\times \left[ 1 - \frac{e^{-2i\theta}}{m\rho^2} + \frac{(1+m)e^{-2i\theta}}{(\rho^2 - m e^{-2i\theta})^2} M(\rho, \theta) \right] \end{aligned} \quad (\text{A6})$$

where

$$\begin{aligned} M(\rho, \theta) &= \frac{\rho^2}{m} (1 - 2m e^{-2i\theta} + m^2) \\ &+ e^{i\theta} (1 - 2m e^{2i\theta} + m^2). \end{aligned} \quad (\text{A7})$$

According to (A6) the deviatoric stress has components

$$s_{\theta\theta} = -s_{\rho\rho} = \frac{1}{2} \text{Re} \mathcal{S}(\rho, \theta); \quad s_{\rho\theta} = \frac{1}{2} \text{Im} \mathcal{S}(\rho, \theta). \quad (\text{A8})$$

Also from Muskhelishvili, the elastic displacement field is:

$$u_\rho^{el} + iu_\theta^{el} = \frac{W\sigma_\infty}{2\mu} F_0(\rho, \theta) F_1(\rho, \theta), \quad (\text{A9})$$

where

$$F_0(\rho, \theta) = \frac{1 - \frac{m}{\rho^2} e^{2i\theta}}{\left(1 - \frac{2m}{\rho^2} \cos 2\theta + \frac{m^2}{\rho^4}\right)^{1/2}}, \quad (\text{A10})$$

and

$$\begin{aligned} F_1(\rho, \theta) &= \frac{\rho}{2} e^{-2i\theta} - \frac{1}{2m\rho} + \frac{e^{-2i\theta}}{4\rho} (\rho^2 e^{2i\theta} - m - 2) \\ &- \frac{e^{-2i\theta} (\rho^2 e^{2i\theta} + m) (\rho^2 e^{-2i\theta} + m + 2)}{4\rho (\rho^2 e^{-2i\theta} - m)} \\ &+ \frac{\rho e^{-2i\theta} (1+m)(1+m^2)}{2m (\rho^2 e^{-2i\theta} - m)}. \end{aligned} \quad (\text{A11})$$

### Acknowledgments

JSL was supported in part by the U.S. Department of Energy, Office of Basic Energy Sciences, Materials Science and Engineering Division, DE-AC05-00OR-22725, through a subcontract from Oak Ridge National Laboratory.



- 
- [1] C.H. Rycroft and E. Bouchbinder, Phys. Rev. Lett. **109**, 194301 (2012).
- [2] J. Ketkaew, W. Chen, H. Wang, A. Datye, M. Fan, G. Pereira, U. Schwartz, Z. Liu, R. Yamada, W. Dmowski, M. Shattuck, C. O'Hern, T. Egami, E. Bouchbinder, and J. Schroers, Nature Communications **9**, 3271 (2018).
- [3] M.L. Falk and J.S. Langer, Phys. Rev. E **57**, 7192 (1998).
- [4] M. L. Falk and J. S. Langer, Annu. Rev. Condens. Matter Phys. **2**, 353 (2011).
- [5] G. Kumar, P. Neibecker, Y. Liu, and J. Schroers, Nature Communications **4**, 1536 (2013).
- [6] J.S. Langer, E. Bouchbinder and T. Lookman, Acta Mat. **58**, 3718 (2010).
- [7] J.S. Langer, Phys. Rev. E **96**, 053005 (2017).
- [8] J.S. Langer, J. Statistical Phys. **175**, 531 (2019).
- [9] J. Fineberg, S.P. Gross, M. Marder, and H.L. Swinney, Phys. Rev. B **45**, 5146 (1992).
- [10] N.I. Muskhelishvili, *Some Basic Problems of the Mathematical Theory of Elasticity*, P. Noordhoff Ltd., Groningen, The Netherlands (1963).
- [11] E. Bouchbinder, J.S. Langer, T.S. Lo, and I. Procaccia, Phys. Rev. E **76**, 026115 (2007).
- [12] J.S. Langer, Phys. Rev. E **62**, 1351 (2000).
- [13] M. Vasoya, C.H. Rycroft and E. Bouchbinder, Phys. Rev. App. **6**, 024008 (2016).
- [14] J.S. Langer, Phys. Rev. E **77**, 021502 (2008).
- [15] J.S. Langer, Phys. Rev. E **92**, 012318 (2015).
- [16] J. Lu, G. Ravichandran, and W. L. Johnson, Acta Mater. **51**, 3429 (2003).
- [17] L. B. Freund, *Dynamic Fracture Mechanics*, Cambridge University Press (1990).
- [18] D.S. Dugdale, J. Mech. Phys. Solids **8**, 100 (1960).
- [19] G.I. Barenblatt, Adv. Appl. Mech. **7**, 56 (1962).
- [20] E.S.C. Ching, J.S. Langer, and H. Nakanishi, Phys. Rev. E **53**, 2864 (1996).
- [21] J.S. Langer and A.E. Lobkovsky, J. Mech. Phys. Solids **46** 1521 (1998).
- [22] E. Bouchbinder, J. Fineberg and M. Marder, Annu. Rev. Condens. Matter Phys. **1**, 371 (2010).
- [23] C.H. Chen, E. Bouchbinder, and A. Karma, Nature Physics **13**, 1186 (2017).
- [24] Y. Lubomirsky, C.H. Chen, A. Karma, and E. Bouchbinder, Phys. Rev. Lett. **121**, 134301 (2018).
- [25] Lawrence E. Malvern, *Introduction to the Mechanics of a Continuous Medium*, Prentice-Hall, Inc., Englewood Cliffs, New Jersey (1969).